Available online at www.sciencedirect.com
ScienceDirect
Polymer 48 (2007) 7614–7622
polymer
www.elsevier.com/locate/polymer

Structural investigation on water-induced phase transitions of poly(ethylene imine), Part IV: Changes of intra- and intermolecular hydrogen bonds in the hydration processes as revealed by time-resolved Raman spectral measurements

Tomoko Hashida, Kohji Tashiro*

Department of Future Industry-oriented Basic Science and Materials, Graduate School of Engineering, Toyota Technological Institute, Tempaku, Nagoya 468-8511, Japan

Received 28 July 2007; received in revised form 19 October 2007; accepted 22 October 2007
Available online 25 October 2007

Abstract

Poly(ethylene imine) (PEI) exhibits water-induced phase transitions among four kinds of crystalline hydrates; anhydrate (EI monomer unit/water molecule = 1/0), hemihydrate (1/0.5), sesquihydrate (1/1.5) and dihydrate (1/2). The chain conformation changes from a double helix in the anhydrate to a planar-zigzag form in the three types of hydrates. Time-resolved Raman spectral measurements have been successfully performed for the first time in the hydration processes of PEI using light and heavy waters. Raman spectral profiles characteristic of each crystal form were obtained in the frequency region of 30–3500 cm^{-1}. Exchange of water from H_2O to D_2O was helpful for shifting the many overlapped bands to identify the characteristic bands. Details of the change in intra- and intermolecular hydrogen bonds have been clarified by quantitative interpretation of the observed Raman spectral data. The conformational disordering occurring in the transition process from the double-stranded helices to the planar-zigzag chains was also discussed.

Keywords: Poly(ethylene imine); Phase transition; Raman spectra

1. Introduction

Linear poly(ethylene imine) [PEI, $-(CH_2CH_2NH)_n-$] exhibits water-induced phase transitions among four kinds of crystalline hydrates depending on the amount of absorbed water; anhydrate (EI monomer unit/water molecule = 1/0), hemihydrate (1/0.5), sesquihydrate (1/1.5) and dihydrate (1/2) as shown in Fig. 1 [1–3]. In this paper these crystalline phases are named anhydrate (0), hemihydrate (0.5), sesquihydrate (1.5) and dihydrate (2) to avoid any confusion in the discussion. The chain conformation changes from a double helix in the anhydrate (0) to a planar-zigzag form in the hemi- (0.5), sesqui- (1.5) and dihydrates (2) [1–3]. The double helix of PEI is formed tightly with the intermolecular N–H···N hydrogen bonds. Once water molecules are absorbed into the lattice, the N–H···O and O–H···N hydrogen bonds are formed between the zigzag-type PEI chains and water molecules. In this way PEI exhibits a remarkable and unique structural change in the water atmosphere. However, the transition mechanism among these PEI hydrates, especially from double helix to a single chain, has not yet been revealed.

PEI has also attracted substantial attention in technological and medical applications. For example, in the field of gene delivery technology a linear PEI is utilized as a vector, which delivers DNA to a target cell because of good compatibility with DNA [4,5]. Since PEI is a weak polyelectrolyte, PEI-

* Corresponding author. Tel.: +81 52 809 1790; fax: +81 52 809 1721.
E-mail address: ktashiro@toyota-ti.ac.jp (K. Tashiro).

0032-3861/$ - see front matter © 2007 Elsevier Ltd. All rights reserved.
doi:10.1016/j.polymer.2007.10.031

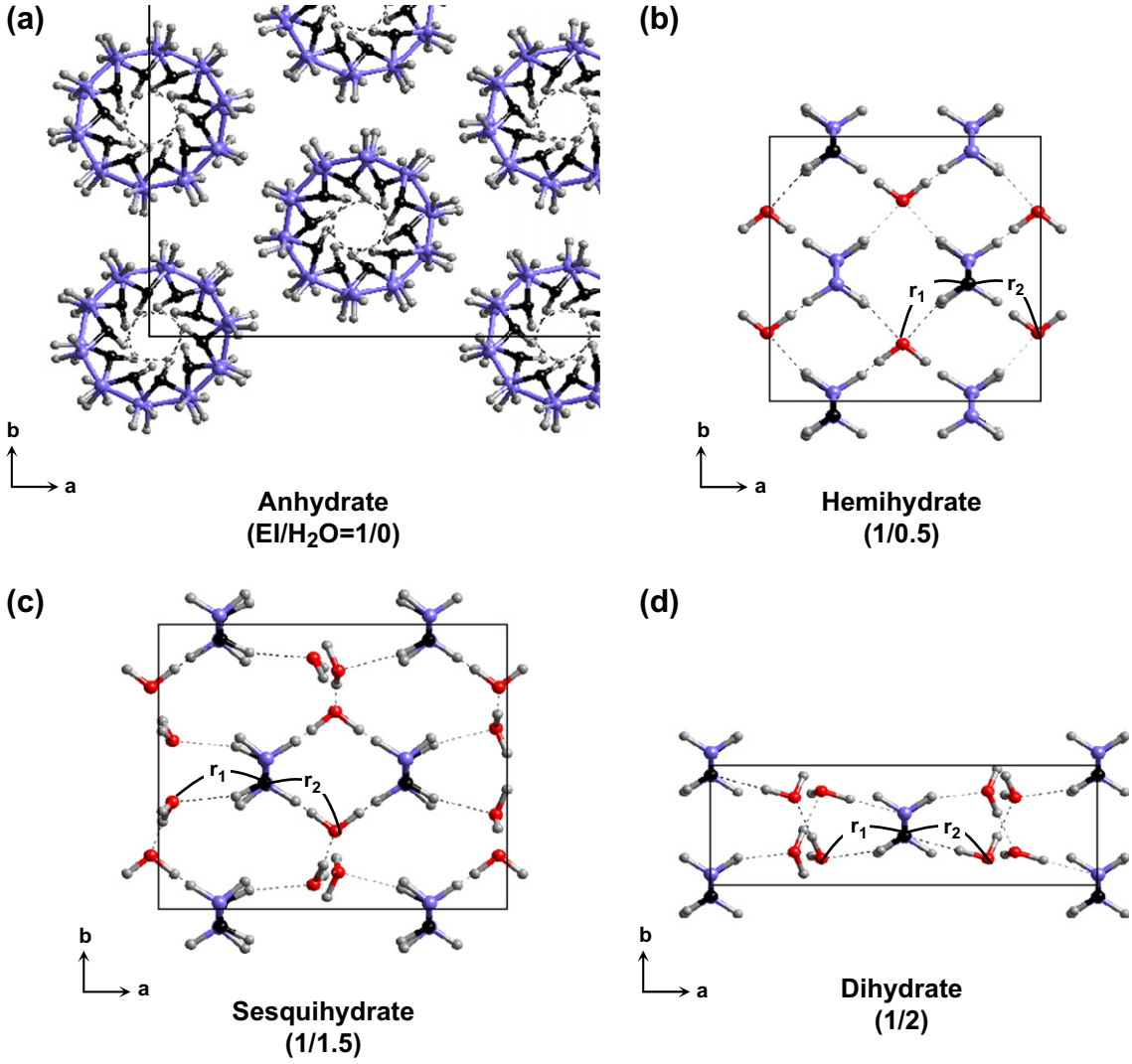

Fig. 1. Crystalline structures of poly(ethylene imine).

metal salt complexes have been studied in association with the ionic conductivity as battery materials [6–8]. It is reported that the ionic conduction of PEI depends on the molecular and crystalline structures, such as the arrangement of NH groups [9] and the hydrogen bonding networks in the hydrates [10]. In this way PEI has been utilized in the extensive application field. But the basic knowledge on the structural features and the transition mechanism of PEI are mostly lacked even now.

In order to reveal the transition mechanism of PEI, we need to study the microscopically-viewed structural change during the phase transitions. In a series of papers [11–13] we have investigated the water-induced phase transition behavior of PEI in the molecular level by utilizing the various techniques including X-ray diffraction and infrared spectroscopy. For example, we have performed the time-resolved measurements of infrared spectra in the hydration process of PEI using both H_2O and D_2O [11]. By analyzing these data we could identify the infrared spectra characteristic of each crystalline phase. The water-induced phase transitions of PEI were found to change quite sensitively depending on temperature as well as relative humidity of the environmental atmosphere. By measuring the humidity and temperature dependence of the infrared spectra, a phase diagram of PEI/water system was proposed [12,13]. However, the microscopically-viewed transition mechanism has not yet been revealed enough well.

Raman spectroscopy is complementary with infrared spectroscopy, and gives us various information which is hard to collect by infrared technique only. For example, the Raman intensity of water bands is much weaker than the corresponding infrared bands. Therefore many bands, which are hidden by the broad and intense water bands in the infrared spectra, may be detected clearly in the Raman bands. It is relatively easy to observe the Raman bands in the low frequency region corresponding to the lattice vibrational modes and the skeletal torsional modes of polymer chains. Raman spectral measurement can be made for any shape of sample, erasing the limitation of the sample in the infrared experiment where the film thickness is limited to several tens of micrometers. In the present study, the time-resolved Raman spectral

measurements have been performed for the first time in the H_2O and D_2O hydration processes of PEI. The thus accumulated Raman data can give us much information useful for the discussion of the structural changes in the phase transition of PEI through the comparison with the previously reported IR data [11].

2. Experimental

Linear PEI was obtained by the alkaline hydrolysis of poly(*N*-acetyl ethylene imine) [M_w: 500,000 g/mol] which was supplied by Dow Chemical Co. Ltd [14,15]. The films cooled from the molten state were dried by evacuation using a rotary pump for 7 days at 30–35 °C to get the anhydrate sample. The thickness of the film used for Raman and wide-angle X-ray diffraction (WAXD) measurements was about 1–2 mm.

To measure the Raman spectra in the hydration process of PEI, an optical cell shown in Fig. 2 was designed. A sample was set on an aluminum plate stored in the cell. The window of the cell was covered with a transparent glass plate.

Time-dependent Raman spectra in the hydration process were measured immediately after the supply of H_2O or D_2O by a syringe. The spectra were measured using a JASCO Raman spectrometer NRS-2100 with a green laser of 532 nm wavelength as an incident beam. The spectral resolution power was 4 cm^{-1}. The Raman spectra were collected at a time interval of 2–5 min in the atmosphere of 100 RH%. In addition the temperature dependence of Raman spectra in the heating process of anhydrate (0) was measured using the hot stage, FDCS196 (Linkam Scientific Instruments Ltd). The sample temperature was kept constant and each Raman spectrum was measured for 5 min. The crystal modification of the sample used in the Raman experiment was checked by measuring the WAXD profile with a Rigaku RINT2000 TTR-III, where the incident beam was a graphite-monochromatized Cu Kα line ($\lambda = 1.5418$ Å). The diffraction profiles were detected with a highly sensitive detector, D/teX.

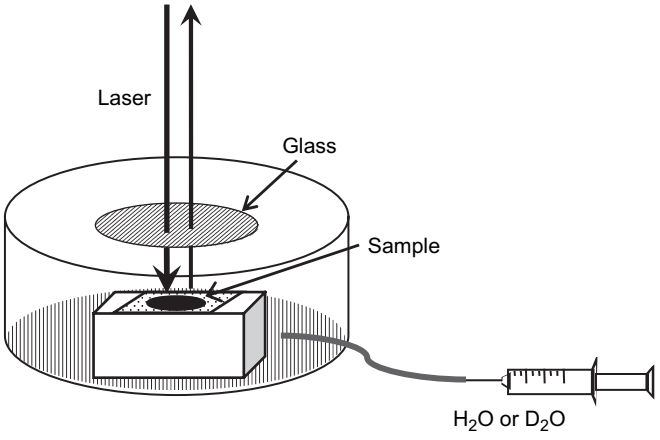

Fig. 2. Optical cell for Raman spectral measurements under a relative humidity.

3. Results and discussion

3.1. Time-dependent Raman spectra in the hydration process

Fig. 3 shows the time-dependent Raman spectra in the frequency region of 750–1580 cm^{-1} during the H_2O hydration process. The spectrum obtained at 0 min corresponds to that of the anhydrate (0). Immediately after injection of water into the cell, the Raman bands of anhydrate (0) (1049, 1109 cm^{-1} and so on) decreased in intensity at first, and the intensity of 1051 cm^{-1} band increased and then decreased. The other new band was detected at 1061 cm^{-1}. The X-ray diffraction measurement revealed that the crystalline phase changed from the anhydrate (0) at the starting point to the dihydrate (2) at the final stage of the experiment. By referring to this X-ray result, the Raman bands may be assigned to each crystalline phase as listed in Table 1. The bands intrinsic to the hemi- (0.5) and sesquihydrates (1.5) were difficult to separate similar to the case of infrared spectra [11]. The band at 1116 cm^{-1} is observed commonly to all the hydrates of 0.5, 1.5 and 2, being assigned to the planar-zigzag conformation.

Fig. 4 shows the time-dependent Raman spectra in the 750–1580 cm^{-1} region, where D_2O was used instead of H_2O. Due to the exchange of NH to ND, many Raman bands were shifted. The observed Raman bands were assigned reasonably to each crystalline phase in a similar way with the above-mentioned H_2O case. The integrated intensities of the thus assigned bands (1049, 1011 and 981 cm^{-1}) are plotted as a function of time in Fig. 5. The 1049 cm^{-1} band of the anhydrate (0) decreased in intensity at first. In parallel the 1011 cm^{-1} band of hemi- (0.5) and sesquihydrates (1.5) increased and then decreased in intensity. Finally the intensity of 981 cm^{-1} band of dihydrate (2) increased.

Figs. 6–8 show the time dependence of Raman spectra during H_2O or D_2O hydration in the frequency region of the stretching modes of CH_2, NH, OH, ND and OD groups. The spectral change in the frequency region of CH_2 stretching mode [$\nu(CH_2)$] was almost common to both H_2O and D_2O hydration processes. The characteristic bands of each hydrate were assigned in a similar manner as shown in Table 1. In the $\nu(CH_2)$ frequency region (Fig. 6) the anhydrate (0) exhibits a complex Raman spectrum including many bands compared with those of the hydrates (0.5, 1.5 and 2). Since the $\nu(CH_2)$ modes are basically localized vibrations, this large difference in the spectra between double helix and zigzag chains was not expected. Possibly the $\nu(CH_2)$ modes are influenced by the torsional angle of polymer skeletal chains, which reflects the complicated molecular structure of double helix.

Table 1 shows the vibrational frequencies of the infrared and Raman bands detected for each crystalline phase, where the tentative assignments of the vibrational modes are also given on the basis of the normal modes calculation results. The details of the normal modes calculation will be reported separately. This table is considered to be quite important for the discussion based on the Raman spectral data on the behavior of PEI in the various phenomena mentioned in Section 1.

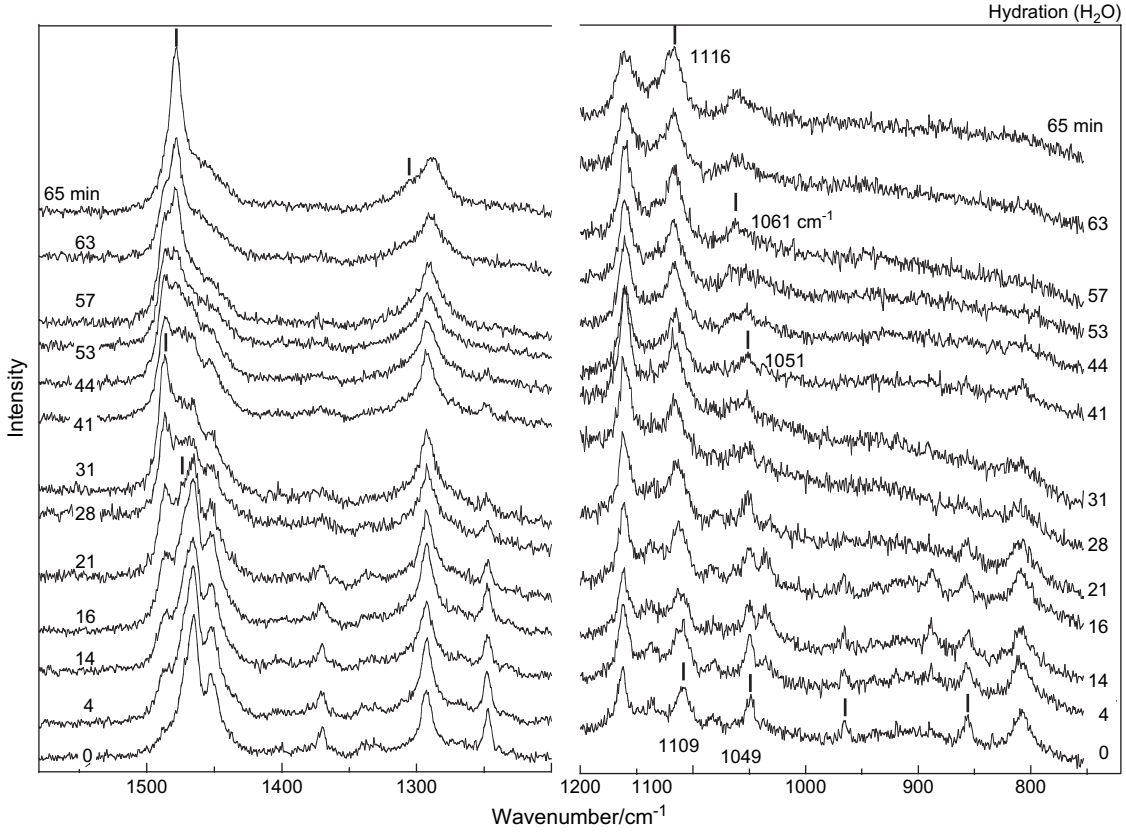

Fig. 3. Time dependence of Raman spectra in the H_2O hydration process in the frequency region of 750–1580 cm^{-1}.

3.2. Intermolecular hydrogen bonds in the water-induced phase transitions

As shown in Fig. 7, the N–H stretching band of the anhydrate (0) appears in relatively low frequency region at 3216 cm^{-1}. The N–H stretching bands of hemi- (0.5) and sesquihydrates (1.5) appear at slightly higher positions of 3273 and 3282 cm^{-1} and those of the dihydrate (2) appear at 3260 and 3271 cm^{-1}. Similar tendency was observed in the D_2O hydration as shown in Fig. 8. Lower frequency shift of N–H stretching mode reflects the stronger hydrogen bonds. The lowest N–H stretching band observed for the anhydrate (0) suggests that the N–H···N hydrogen bond between the chains of the double helix is very strong. When the sample absorbs water, the N–H···O, O–H···N and O–H···O hydrogen bonds are formed among PEI chains and water molecules and the molecular conformation of PEI changes to a planar-zigzag form.

Table 2 shows the vibrational frequencies of the N–H and O–H stretching bands observed for the various hydrates. Since the N–H band frequency of dihydrate (2) is lower than that of hemi- (0.5) and sesquihydrates (1.5), the N–H···O hydrogen bonds of the dihydrate (2) are considered to be stronger than those of the hemi- (0.5) and sesquihydrate (1.5). As for the O–H···N and O–H···O hydrogen bonds, the O–H stretching bands observed in the infrared spectra give us useful information as shown in Fig. 9. The intensity of O–H stretching band at 3115 cm^{-1} is stronger for the hemi- (0.5) and sesquihydrates (1.5) and the 3375 cm^{-1} band intensity is stronger for the dihydrate (2). These bands are assigned to the O–H stretching modes of water molecules existing in the hydrates, where both of the O–H···N and O–H···O hydrogen bonds are included. From the relative position of the O–H stretching bands, the O–H···N and O–H···O hydrogen bonds are considered to be stronger in the hemi- (0.5) and sesquihydrates (1.5) than in the dihydrate (2).

Chatani et al. estimated the hydrogen bond distances for all the hydrates on the basis of X-ray structural analysis [1–3]. The N···N interatomic distances along the N–H···N hydrogen bonds in the anhydrate (0) are 3.10 and 3.16 Å, which is rather shorter than the sum of the van der Waals radii of N, H and N atoms ($1.55 + 1.2 + 1.55 = 4.3$ Å), indicating the strong hydrogen bonds as speculated from the Raman spectra mentioned above. Because of this strong bond between the NH groups, the double helix of the anhydrate (0) is considered to be stabilized energetically. The N···O interatomic distances in the hydrates are reported to be 3.05 Å (r_1 in Fig. 1) and 2.87 Å (r_2) for the hemihydrate (0.5), 2.96 Å (r_1) and 2.93 Å (r_2) for the sesquihydrate (1.5), and 2.93 Å (r_1 and r_2) for the dihydrate (2). The r_1 becomes shorter as the structure changes from hemi- (0.5) to sesqui- (1.5) and to dihydrate (2): 3.05 Å (0.5) → 2.96 Å (1.5) → 2.93 Å (2). On the other hand, the r_2 becomes longer by hydration: 2.87 Å (0.5) → 2.93 Å (1.5) → 2.93 Å (2). As shown in Table 2, the changes in N···O interatomic distances (r_1 and r_2) are consistent with the changes in the vibrational frequencies of the related bands.

Table 1
Observed infrared and Raman bands characteristic of the crystalline phases of poly(ethylene imine)[a]

H_2O								
Anhydrate (0)		Hemi (0.5)		Sesqui (1.5)		Di (2)		Approximate assignment[b]
IR	Raman	IR	Raman	IR	Raman	IR	Raman	
	113		74		74		50	Lattice vibrations + ν(CC, CN)
	330							+ δ(CCN, CNC)
	549							
		693		693				r(OH)
800		755		755		850		r(NH), r(CH_2)
856	856	824		824		918		
883	966	875		874				
	1049	1046	1051	1046	1051	1048	1061	ν(CC), ν(CN)
	1109					1130	1116	
	1163	1138	1116	1138	1116			
1246		1204		1200				
1281		1277		1275		1282	1305	w(NH), w(CH_2), t(CH_2)
1291		1289		1289				
1330		1305						
1333								
1447								
1471		1458	1474	1457	1474	1475	1478	δ(NH), δ(CH_2)
1492		1486	1487	1486	1487	1486		
1499								
		1652		1652		1652		δ(OH)
2655	2657							
2688	2731		2744		2744		2755	
2734	2811	2846	2851	2846	2851	2846	2858	
2810	2877	2911	2892	2911	2892	2911	2897	
2878	2908							ν(CH_2)
2916	2929							
		3115		3115				ν(NH), ν(OH)
3219	3216	3271	3273	3271	3273	3265	3260	
		3280	3282	3280	3282	3375	3271	

D_2O						
Hemi (0.5)		Sesqui (1.5)		Di (2)		Approximate assignment[b]
IR	Raman	IR	Raman	IR	Raman	
	74		74		50	Lattice vibrations + ν(CC, CN)
						+ δ(CCN, CNC)
681		661				r(ND), r(CH_2)
822		840		730		
		881		846	871	
	927	924	927	965	981	
1091	1011	1087	1011	1121	1057	ν(CC), ν(CN)
1124	1113	1112	1113			
1191		1191		1191		δ(OD)
	1147		1147		1147	w(CH_2), w(ND), t(CH_2)
1332	1281	1347	1281	1319	1260	
1349				1356		
1447		1448		1413		δ(CH_2)
	1474	1472	1474	1476	1478	
	1487		1487	1487		
2355	2428	2200		2200	2394	ν(ND), ν(OD)
2386	2444	2355	2428	2420	2427	
		2396	2444	2500		
		2500				
2685	2744	2683	2744		2755	ν(CH_2)
2846	2851	2846	2851	2846	2858	
2911	2892	2911	2892	2911	2897	

[a] The values are in unit of cm^{-1}.
[b] ν: stretching mode, δ: bending mode, r: rocking mode, w: wagging mode, t: twisting mode.

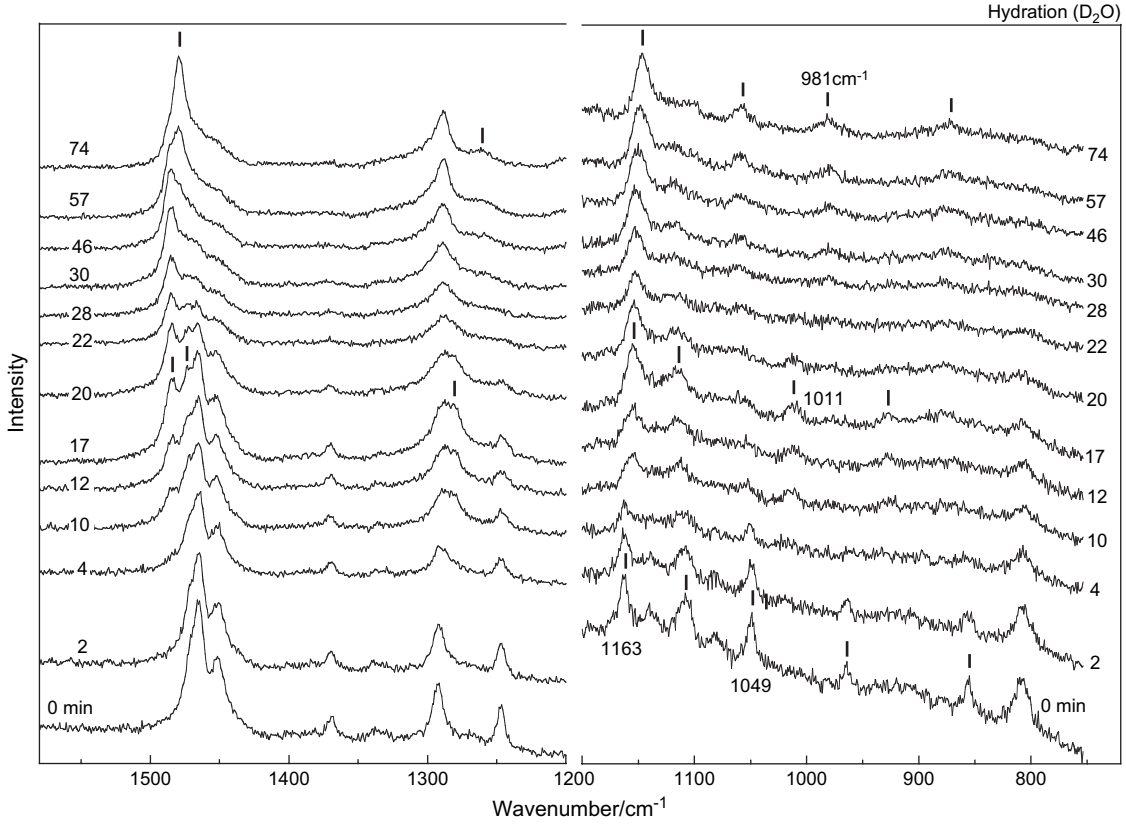

Fig. 4. Time dependence of Raman spectra in the D_2O hydration process in the frequency region of 750–1580 cm^{-1}.

As reported in the previous work [13], the melting point of hydrates is 60 °C for the anhydrate (0), 70–90 °C for the hemi- and sesquihydrate (0.5, 1.5), 90–110 °C for the dihydrate (2). The strongest N–H···O hydrogen bonds in the dihydrate (2) are considered to contribute to the highest thermal stability of the crystalline phase. The N–H···N hydrogen bonds inside the double helix are very strong as mentioned

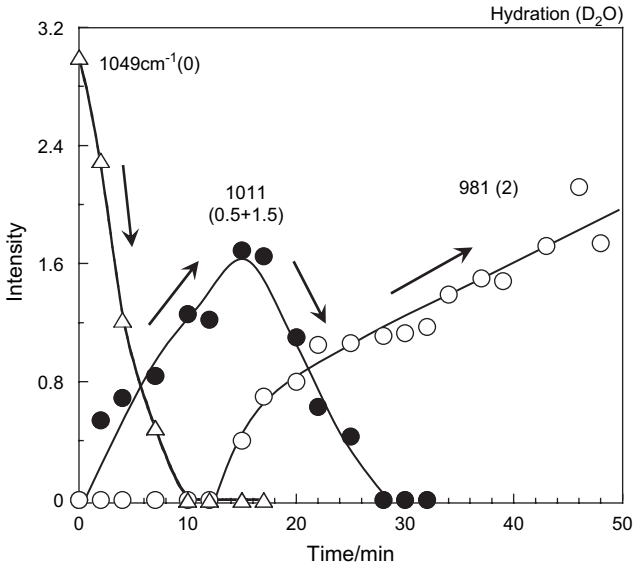

Fig. 5. Integrated intensity of the Raman bands intrinsic of the hydrates as a function of time in the D_2O hydration process.

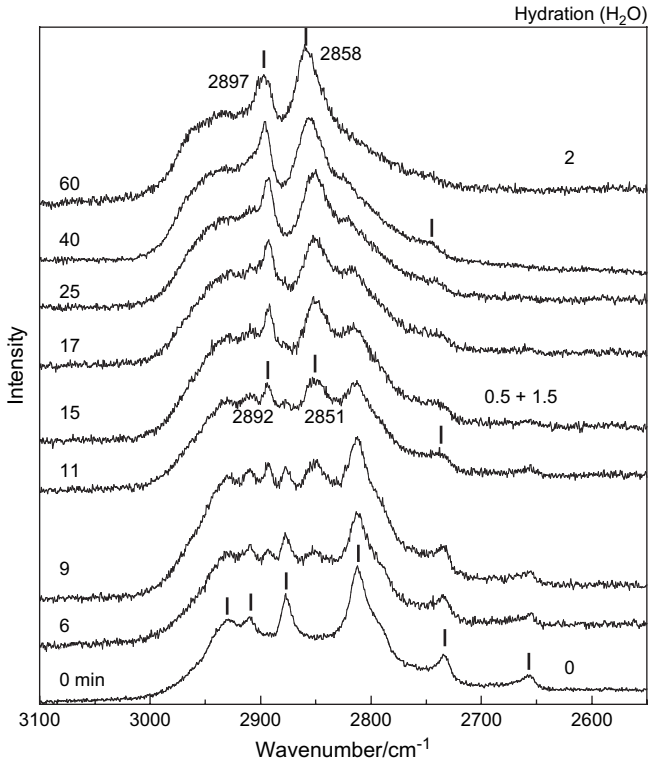

Fig. 6. Time dependence of Raman spectra in the frequency region of 2550–3100 cm^{-1} in the H_2O hydration process.

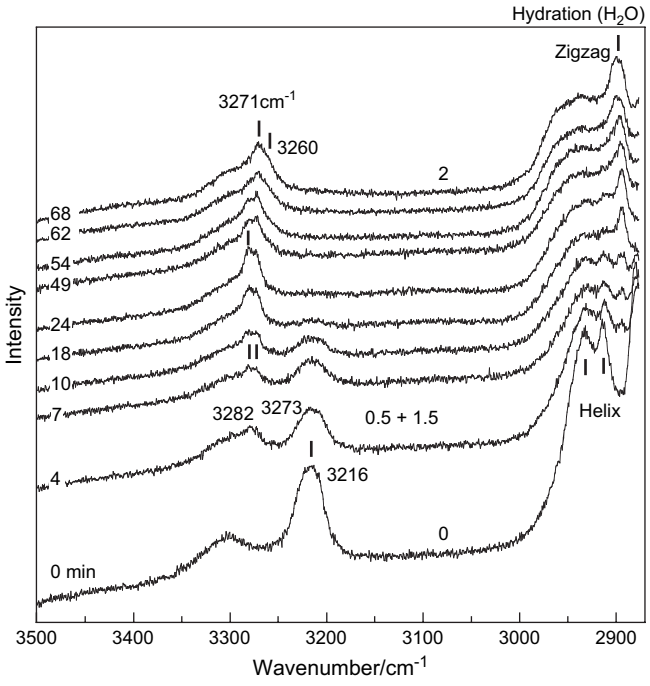

Fig. 7. Time dependence of Raman spectra in the frequency region of 2870–3500 cm^{-1} in the H_2O hydration process.

above, but the packing of double helices in the crystal lattice is kept by weak van der Waals interactions. Therefore, the melting temperature of the anhydrate (0) is the lowest among the hydrates.

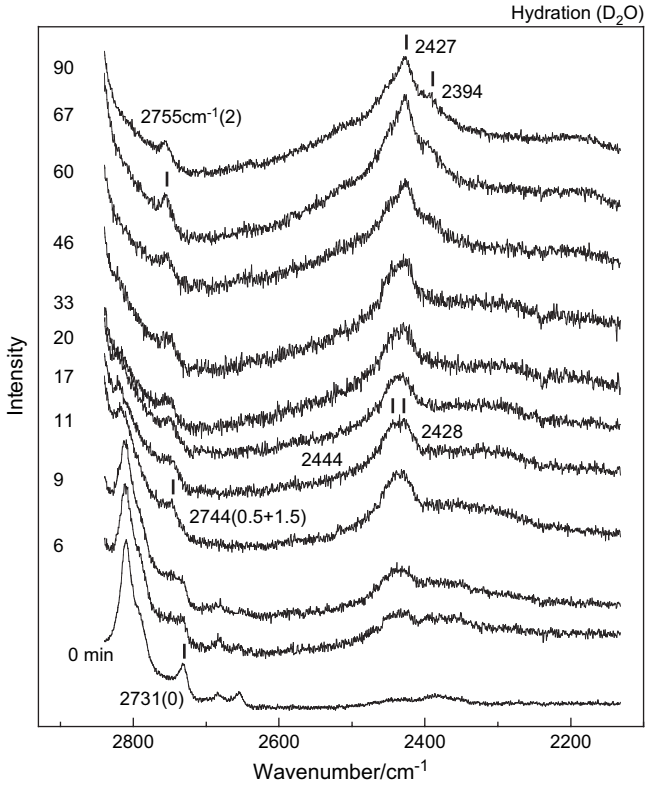

Fig. 8. Time dependence of Raman spectra in the frequency region of 2130–2830 cm^{-1} in the D_2O hydration process.

Table 2
The correlation between the vibrational frequencies of the infrared and Raman bands and the geometrical changes in the PEI hydrates

Hydrogen bonds	Hydrates	Raman (cm^{-1})	IR (cm^{-1})	H-bond strength	N···O distance (Å)
N–H···N	0	3216	3219	Strong	3.10, 3.16
N–H···O	0.5	3273, 3282	3271, 3280	Weaker	3.05 (r_1)[a]
N–H···O	1.5	3273, 3282	3271, 3280	∧	2.96 (r_1)
N–H···O	2	3260, 3271	3265	Stronger	2.93 (r_1)
O–H···N	0.5	–	3115	Stronger	2.87 (r_2)
O–H···N	1.5	–	3115	∨	2.93 (r_2)
O–H···N	2	–	3375	Weaker	2.93 (r_2)

[a] r_1 and r_2: refer to Fig. 1.

3.3. Time-dependent Raman spectra in the low frequency region during the hydration process

Raman spectra in the low frequency region of 30–600 cm^{-1} were measured during the hydration process as shown in Fig. 10. The spectral change in this frequency region was common to the H_2O and D_2O cases. The spectrum at 0 min corresponds to that of the anhydrate (0). With absorbing water, the anhydrate (0) bands at 113 and 549 cm^{-1} decrease in intensity and the band at 74 cm^{-1} of the hemi- (0.5) and sesquihydrates (1.5) appears and increases in intensity. As the intensity of the 74 cm^{-1} band (0.5 + 1.5) decreases again, the band at 50 cm^{-1} of the dihydrate (2) starts to increase. These Raman bands relate with the lattice modes and the torsional and bending modes of the skeletal chains, reflecting the remarkable changes in the molecular chain conformation and the chain packing mode during this phase transition.

Fig. 11 shows the temperature dependence of Raman spectra in the heating process of the anhydrate (0). The intensity and half-width of 549 cm^{-1} band are plotted as a function of temperature as shown in Fig. 12. In the temperature region of 40–60 °C before the melt of anhydrate (0), the half-width of 549 cm^{-1}

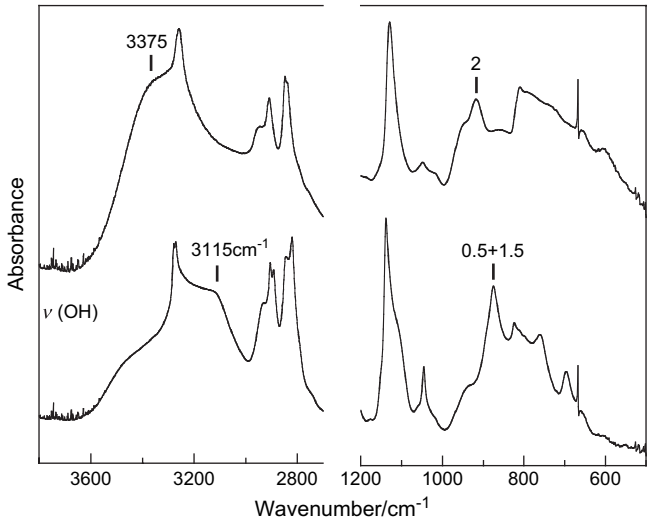

Fig. 9. Infrared spectra characteristic of the hemi- (0.5) and sesquihydrates (1.5) and the dihydrate (2) in the H_2O hydration.

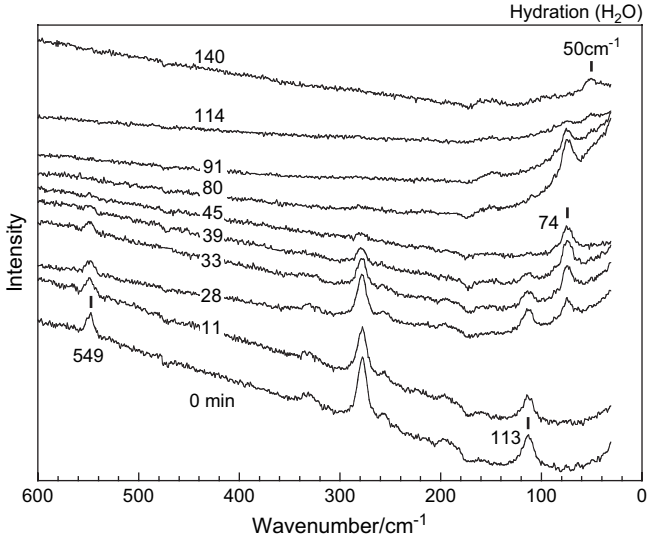

Fig. 10. Time dependence of Raman spectra in the frequency region of 30–600 cm^{-1} in the H_2O hydration process.

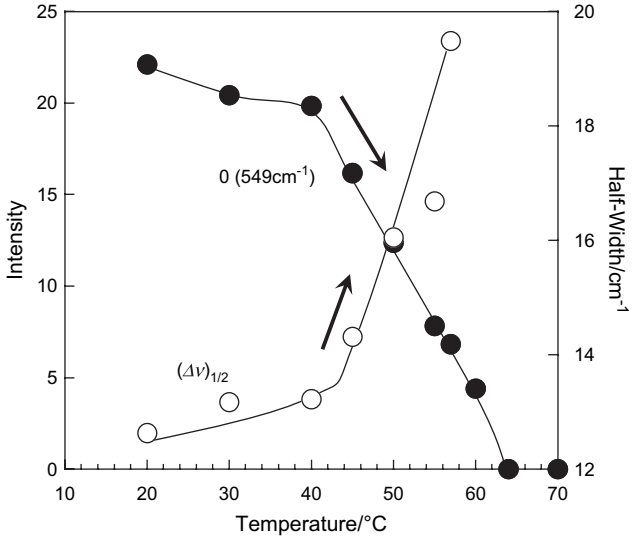

Fig. 12. Integrated intensity and half-width of 549 cm^{-1} (0) band as a function of temperature.

band increases largely. According to the normal modes calculation made for anhydrate (0), the 549 cm^{-1} band is tentatively assigned to the bending mode of the skeletal chains (the details of the calculation will be reported elsewhere). Therefore, this band broadening could be caused by the conformational disorder of skeletal chains of the double helix.

Similar behavior can be detected also in the hydration process from the anhydrate (0) to the hydrates as shown in Fig. 10. Before the disappearance of the 549 cm^{-1} anhydrate band, the shape of the band becomes broader. The intensity and half-width of 549 cm^{-1} band (0) and the intensity of 74 cm^{-1} band (0.5 + 1.5) are plotted against time as shown in Fig. 13. As the 549 cm^{-1} band (0) decreases in intensity, the corresponding half-width increases, during which the anhydrate (0) transfers to the hemi- (0.5) and sesquihydrates

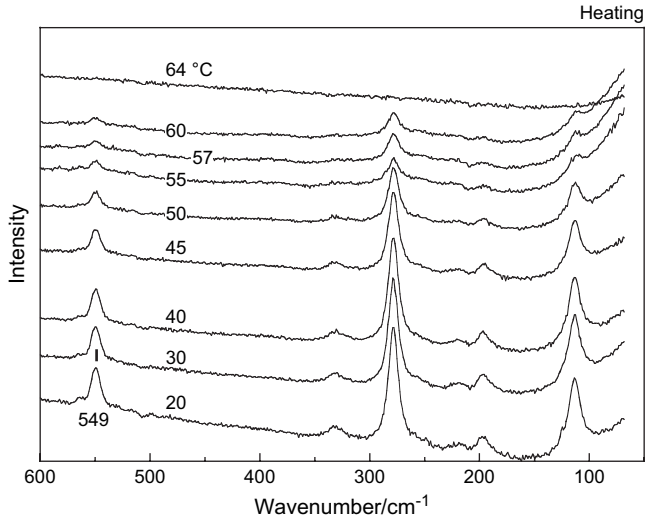

Fig. 11. Temperature dependence of Raman spectra in the heating process of the anhydrate (0) in the frequency region of 30–600 cm^{-1}.

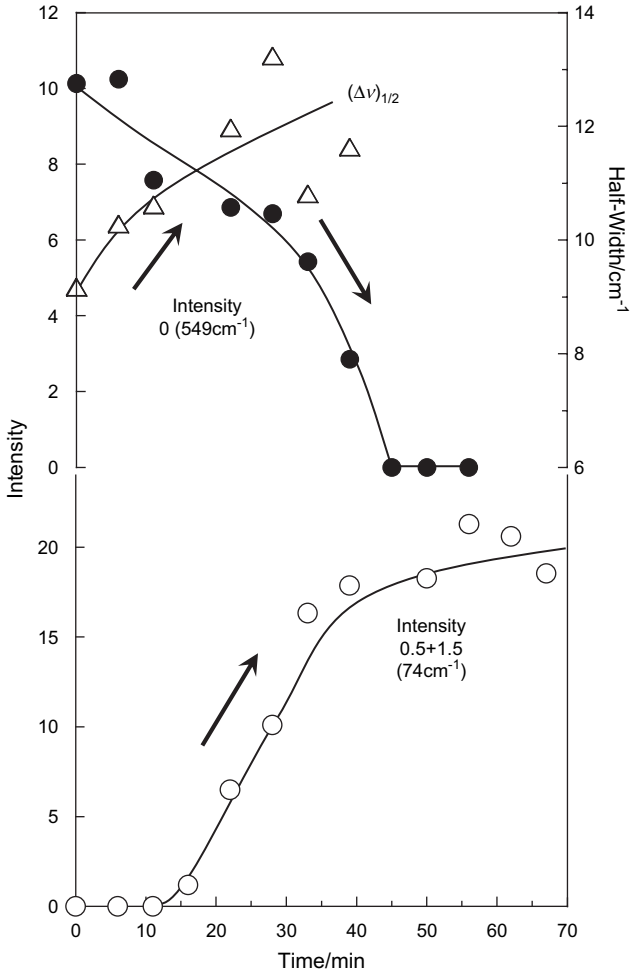

Fig. 13. Integrated intensity and half-width of 549 cm^{-1} (0) band and the intensity of 74 cm^{-1} (0.5 + 1.5) band as a function of time in the H_2O hydration process.

(1.5). These observations allow us to speculate that the mobility of skeletal chains is enhanced and the helical chains become disordered more or less, just when the double helix is loosened to the separated planar-zigzag chains.

4. Conclusion

Time dependence of Raman spectra in the water-induced phase transitions of PEI has been successfully measured during the H_2O and D_2O hydration. The utilization of D_2O helped the band assignment to each crystalline form by shifting the bands through the H–D exchange. The Raman bands characteristic of anhydrate (0) and hydrates were identified in the frequency region of 30–3500 cm^{-1} as listed in Table 1. On the basis of this information the characteristic features of hydrogen bonds have been investigated. By comparing the positions of the bands related with the N–H and O–H stretching modes, we could estimate the relative strength of the hydrogen bonds. The N–H···N hydrogen bond of the anhydrate (0) is strong. The hydrogen bond of N–H···O is stronger in the dihydrate (2) than in the hemi- (0.5) and sesquihydrates (1.5). Similarly, comparing the infrared O–H stretching bands intrinsic of the hydrates, the O–H···N and O–H···O hydrogen bonds are found to be stronger in the hemi- (0.5) and sesquihydrates (1.5) than in the dihydrate (2).

Raman spectral changes in the low frequency region were also measured during the hydration process. In particular the 549 cm^{-1} band characteristic of the anhydrate (0) shows remarkable change in the phase transition. That is, the half-width increases remarkably, suggesting an occurrence of active motion of the skeletal chains in the transformation process from the double helix to the isolated zigzag chains. The band assignments presented in Table 1 are needed to be confirmed by performing the normal modes calculation for the various hydrates including water molecules.

Acknowledgement

This work was financially supported by the MEXT "Collaboration with Local Communities" project (2005–2009) and the Sasakawa Scientific Research Grant from the Japan Science Society.

References

[1] Chatani Y, Tadokoro H, Saegusa T, Ikeda H. Macromolecules 1981; 14:315.
[2] Chatani Y, Kobatake T, Tadokoro H, Tanaka R. Macromolecules 1982; 15:170.
[3] Chatani Y, Kobatake T, Tadokoro H. Macromolecules 1983;16:199.
[4] Rudolph C, Muller RH, Rosenecker JJ. Gene Medicine 2002;4:66.
[5] Trubetskoy VS, Wong SC, Subbotin V, Budker VG, Loomis A, Hangstrom JE, et al. Gene Therapy 2003;10:261.
[6] Harris CS, Ratner MA, Shriver DF. Macromolecules 1987;20:1778.
[7] Costantino U, Caciola M, Pani G, Jones DJ. Solid State Ionics 1997; 97:261.
[8] York SS, Buckner M, Frech R. Macromolecules 2004;37:994.
[9] Borkovec M, Koper GMJ. Macromolecules 1997;30:2151.
[10] Watanabe M, Ikezawa R, Sanui K, Ogata N. Macromolecules 1987;20: 968.
[11] Hashida T, Tashiro K, Aoshima S, Inaki Y. Macromolecules 2002; 35:4330.
[12] Hashida T, Tashiro K, Inaki Y. Polymer 2003;44:1721.
[13] Hashida T, Tashiro K, Inaki Y. Journal of Polymer Science, Part B: Polymer Physics 2003;41:2937.
[14] Saegusa T, Ikeda H, Fujii H. Polymer Journal 1972;3:35.
[15] Saegusa T, Ikeda H, Fujii H. Macromolecules 1972;5:359.